Pergamon

Int. J. Solids Structures Vol. 32, No. 19, pp. 2907–2922, 1995

0020-7683/95 $9.50 + .00

0020-7683(94)00241-X

FRACTAL MODELS OF ELASTIC–PERFECTLY PLASTIC CONTACT OF ROUGH SURFACES BASED ON THE CANTOR SET

THOMAS L. WARREN and DUSAN KRAJCINOVIC
Department of Mechanical and Aerospace Engineering, Arizona State University, Tempe, AZ 85287-6106, U.S.A.

(*Received* 16 *December* 1993; *in revised form* 21 *September* 1994)

Abstract—The objective of this study was to formulate discrete and continuous models to describe the elastic–perfectly plastic deformation of two rough surfaces in contact. The two surfaces in contact are assumed to exhibit fractal behavior and are modeled as an effective fractal surface compressed into a smooth rigid substrate. The rough self-affine fractal structure of the effective surface is approximated using a Cantor set representation. Both of the proposed models admit analytical solutions for the cases when the plastic deformation is volume conserving or not. Results are presented that illustrate the effects that volume conservation and initial surface structure have on the elastic–perfectly plastic deformation process. The results from the continuous model are compared with the results obtained from the discrete model, and also with existing experimental load displacement results for the deformation of a ground steel surface.

1. INTRODUCTION

It is well known that the geometry and structure of the interface between two solid surfaces in contact is of fundamental importance to the study of friction, wear, lubrication, and also thermal and electrical conductivity. In general, the actual contact between two real solids is realized only over a small fraction of surface in a discrete number of areas. Consequently, the real area of contact is only a fraction of the apparent (nominal) area, and the parameters of the actual contact regions depend upon the curvature and roughness of the contacting surfaces. Early studies of the contact of rough surfaces are described in Archard (1957), Bowden and Tabor (1964), and Greenwood and Williamson (1966). More recent studies are available in Johnson (1985), Liu *et al.* (1986), Chang *et al.* (1987), Bhushan (1990), Majumdar and Bhushan (1991), Majumdar *et al.* (1991), Borodich and Mosolov (1991,1992), Bhushan and Majumdar (1992) and Warren *et al.* (1994).

In most cases the structure of surfaces appears to be random. Statistical parameters such as the root-mean square (r.m.s.) of surface height σ, slope σ' and curvature σ'' are conventionally used to characterize the surface roughness. Several theories based on these parameters have been developed to model rough surfaces in contact. The most popular of these is the Greenwood and Williamson (G & W) (1966) model, which is based on the assumption that the surface is composed of hemispherical asperities having equal radii of $1/\sigma''$. The centers of asperities are distributed normally about the mean plane, and the deformation of the asperities is based on the Hertz contact theory. Recently, Chang *et al.* (1987) modified the original G&W model to incorporate the effects of volume conservation in the plastic deformation of asperities. Several other theories of friction, wear, and lubrication based on the G&W model have since been developed and are discussed by Bhushan (1990). However, as pointed out by Majumdar and Bhushan (1991), Majumdar *et al.* (1991), and Bhushan and Majumdar (1992), the parameters σ, σ', and σ'' are not unique to a surface, and depend upon the resolution and scan length of the roughness measuring instrument. Because of this fact, the assumption of a surface composed of hemispherical asperities, belonging to a single length scale, is an oversimplification of the real surface which contains several roughness scales.

The multi-scale nature of the surface roughness suggests the use of a fractal representation. Lately (Liu *et al.*, 1986; Majumdar and Bhushan, 1991; Majumdar *et al.*, 1991;

Borodich and Mosolov, 1991,1992; Bhushan and Majumdar, 1992; Warren *et al.* 1994), fractal models have indeed been used to represent the contact of rough surfaces. The method developed by Majumdar and Bhushan (1991), Majumdar *et al.* (1991), and Bhushan and Majumdar (1992) uses the Weierstrass–Mandelbrot function, as described by Mandelbrot (1982), to simulate surface roughness. Modified Hertz equations are then employed to model the elasto–plastic deformation of the surface. In Liu *et al.* (1986), a fractal surface is constructed based on a Cantor set that is used to simulate the electrical properties exhibited by a rough surface interface. The model developed by Borodich and Mosolov (1991,1992), also based on the Cantor set, is used to provide asymptotic expressions for a fractal die penetrating either a rigid–perfectly plastic, or elastic halfspace. Hill's solution (Hill, 1950) for a punch in contact with a rigid perfectly plastic halfspace is employed to estimate plastic deformation. For elastic deformation, the surface of the halfspace is modeled using a Winkler foundation (Cook and Young, 1985) which corresponds to a distribution of mutually independent linear springs. The Borodich and Mosolov model was subsequently modified by Warren *et al.* (1994) to describe the plastic deformation of a fractal surface, and incorporate the effects of volume conservation. With this model each asperity is idealized as a simple one-dimensional axially loaded column which is composed of a rigid–perfectly plastic material that deforms when a critical load is reached.

It is shown by Johnson (1985) and Majumdar *et al.* (1991) that the contact between two rough surfaces can be modeled as the contact of an effective surface with a rigid flat surface. Because of this fact, it is of interest to obtain a solution for the deformation of an equivalent surface generated with a Cantor set. In this paper, the method used by Warren *et al.* (1994) is modified assuming that an elastic–perfectly plastic fractal surface is in contact with a smooth, rigid, and frictionless halfspace. Within the framework of this refined model each asperity is treated as a simple one-dimensional axially loaded column made of an elastic–perfectly plastic material. The volume of the plastically deforming material is conserved throughout the plastic deformation phase assuming that the plastically deformed material flows into specific regions of the Cantor set structure.

2. CHARACTERIZATION OF A FRACTAL SURFACE

Using the method developed by Borodich and Mosolov (1991,1992), and modified by Warren *et al.* (1994), the surface profile shown in Fig. 1 is constructed by joining the segments obtained at successive stages of the Cantor set. At each stage of construction, the middle sections of the initial segments are removed so that the lengths of the remaining segments are $1/f_x$ times the length of the initial segments, where $f_x > 1$. The depth of the recesses (measured from the last step) at the $(n+1)$th construction step of the fractal surface is $1/f_z$ times less than the depth at the nth step, where $f_z > 1$. From this result, it can easily be shown that the horizontal length and recess depth of the $(n+1)$th step are, respectively,

$$L_{n+1} = \left(\frac{1}{f_x}\right)L_n = \left(\frac{1}{f_x}\right)^{n+1} L_0 \quad \text{and} \quad h_{n+1} = \left(\frac{1}{f_z}\right)h_n = \left(\frac{1}{f_z}\right)^{n+1} h_0. \tag{1}$$

Most rough surfaces have a self-affine scaling structure (Majumdar *et al.*, 1991), which implies that the length scales change by different amounts in different directions. This is also evident with the case of the structure constructed in Fig. 1. Because of this fact, methods used for self-similar fractals are not applicable to self-affine structures as described by Mandelbrot (1985). However, a relationship between the self-affine Cantor set structure and a self-affine surface $z(x)$ is conjectured through the use of the structure function

$$S(\tau) = \langle [z(x+\tau) - z(x)]^2 \rangle, \tag{2}$$

where $S(\tau)$ physically represents the mean square of the difference in height expected over any spatial distance τ, and the angular brackets denote averaging over the statistical ensemble of $z(x)$. It has been shown by Voss (1988) that the structure function scales as

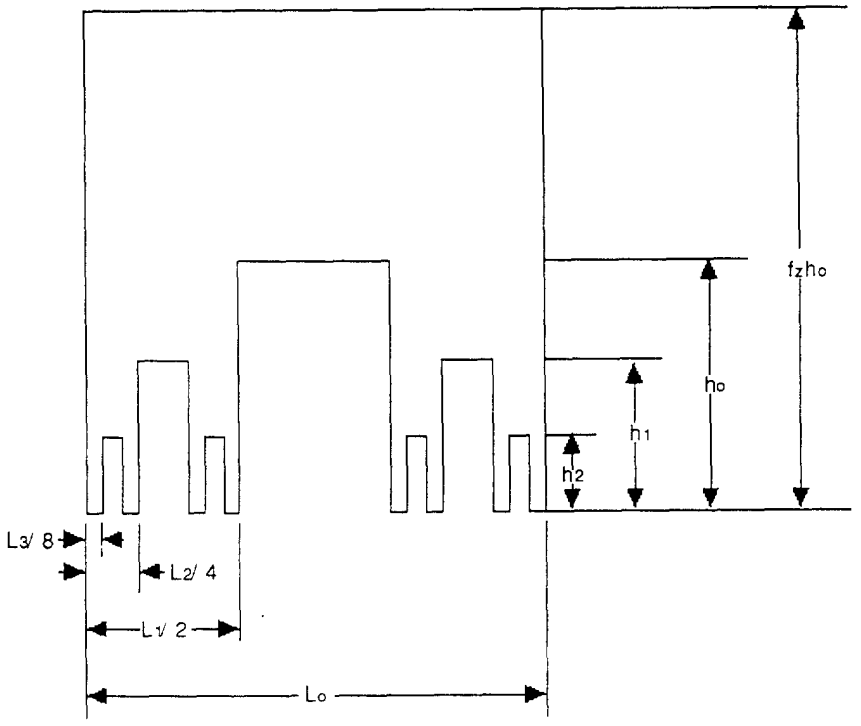

Fig. 1. Fractal surface constructed from the Cantor set with $s = 2$.

$$S(\tau) \sim \tau^{4-2D}, \tag{3}$$

where D is the self-affine fractal dimension of the surface profile, which falls in the range $1 < D < 2$. From eqns (2) and (3), it follows that

$$\Delta z \sim \Delta x^{2-D}, \tag{4}$$

where $(2-D)$ is equivalent to the well-known Hurst exponent.

It was shown by Borodich and Mosolov (1992), that a self-affine fractal dimension for the Cantor set structure (Fig. 1) can be obtained based on certain statistical considerations. At the nth generation, the Cantor set surface contains $N = s^n$ segments, each of length

$$\delta_n = \left(\frac{1}{sf_x}\right)^n L_0, \tag{5}$$

where s corresponds to the number of asperities on a repeating segment (Warren *et al.*, 1994). This result allows for the construction of an infinite number of different structures based on the Cantor set.

During an iterational step in the construction of the Cantor set surface, scaling in the horizontal direction requires

$$\Delta x_{n+1} = \left(\frac{1}{sf_x}\right)\Delta x_n. \tag{6}$$

In the vertical direction, the corresponding fluctuations Δz_n at the nth generation can be obtained by considering the probability of finding the value

$$z_n = \left(\frac{1}{f_z}\right)^n h_0. \tag{7}$$

The actual construction of the self-affine Cantor set profile is based on deterministic methods, while its relationship to a surface profile exhibiting fractional Brownian motion is based on statistical considerations. At the nth generation, the support of eqn (7) has a total length $(L_n - L_{n+1})$, from which the probability of finding z_n is $P(z_n) = (L_n - L_{n+1})/L_0$. Hence,

$$P(z_n) = \left(\frac{1}{f_x}\right)^n \left(1 - \frac{1}{f_x}\right). \tag{8}$$

As shown by Borodich and Mosolov (1992), the fluctuation Δz_n at the nth generation can be obtained by assuming that Δz_n scales as the expected value $z_n P(z_n)$ in which

$$\Delta z_n \sim z_n P(z_n). \tag{9}$$

Thus, the expected value of the fluctuation at the $(n+1)$th generation is related to the expected value of the fluctuation at the nth generation through the relationship

$$z_{n+1} P(z_{n+1}) = \left(\frac{1}{f_z f_x}\right) z_n P(z_n). \tag{10}$$

Hence

$$\Delta z_{n+1} = \left(\frac{1}{f_z f_x}\right) \Delta z_n. \tag{11}$$

Using eqns (6) and (11) in eqn (4) provides the relationship

$$\left(\frac{\Delta z_{n+1}}{\Delta z_n}\right) = \left(\frac{\Delta x_{n+1}}{\Delta x_n}\right)^{2-D}, \tag{12}$$

from which the self-affine fractal dimension for the Cantor set surface is derived as

$$D = 1 - \frac{\ln f_z}{\ln s f_x} + \frac{\ln s}{\ln s f_x}, \quad (1 < D < 2). \tag{13}$$

It is interesting to note that the last term on the right-hand side of eqn (13) provides the fractal dimension of the Cantor set D_c, $(0 < D_c < 1)$.

The fractal dimension D along with the parameters L_0 and h_0 can be determined experimentally from a surface profile of a material specimen. The fractal dimension D can be directly obtained from the gradient of the structure function of a surface profile that exhibits fractional Brownian motion, while L_0 corresponds to the profile length, and h_0 is equal to twice the r.m.s. height σ. The self-affine fractal dimension of the material specimen is related to the self-affine fractal dimension of the Cantor set structure through the three geometric parameters s, f_z, and f_x as given in eqn (13). A unique choice of the three unknown geometric parameters requires two more equations. The two other relationships for the parameters f_z and f_x can be obtained by considering the linear area that is in contact with a plane intersecting the experimentally obtained surface profile at two separate

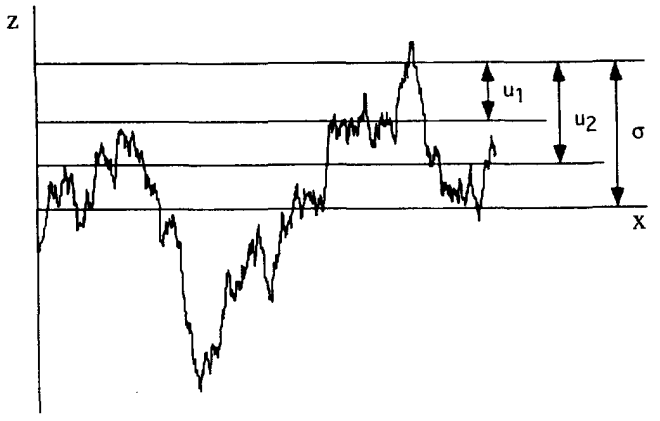

Fig. 2. Fractal surface profile intersected by two planes below the r.m.s. height σ.

locations as shown in Fig. 2. These linear areas can be equated to the linear areas computed from the asymptotic results for the area displacement relationship neglecting volume conservation (Warren *et al.*, 1994) given by eqn (A7) in the Appendix. Thus the proposed model in conjunction with experimental measurements provides a unique, if only approximate, selection of all three parameters needed to define the Cantor set structure.

3. DISCRETE ELASTIC–PERFECTLY PLASTIC DEFORMATION MODEL

The proposed fractal surface model is assumed to be a semi-infinite solid composed of an elastic–perfectly plastic material. The fractal surface of this body is assumed to be in contact with a smooth rigid halfspace as shown in Fig. 3. Deformation of each generation of asperities is initially elastic. After a critical load (per unit thickness)

$$P = \sigma_y L \tag{14}$$

is reached, the deformation becomes plastic. In eqn (14), σ_y is the local value of the yield stress of the deforming elastic–perfectly plastic material in compression, and L is the length of contact between the deforming material and the rigid halfspace. The local value of yield stress implies the stress required to produce plastic deformation at the length scale under consideration, and may be different from the value used at the macro scale.

The total elastic deformation of the Cantor set surface can be determined by superimposing the elastic deformation of each generation of asperities such that

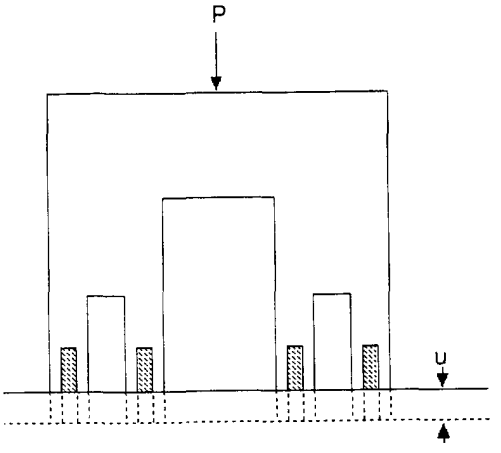

Fig. 3. Deforming Cantor set surface with $s = 2$.

$$u_e = P \sum_{i=0}^{n} \frac{z_i}{A_i E_i}, \tag{15}$$

where z_i, A_i, and E_i are the height, total cross-sectional area (per unit thickness), and Young's modulus, respectively, of the ith generation of asperities. In terms of the parameters L_0, h_0, f_x, and f_z, the height and cross-sectional area for the ith generation of asperities are given, respectively, by

$$z_i = \left(\frac{1}{f_z}\right)^i (f_z - 1)h_0, \quad A_i = \left(\frac{1}{f_x}\right)^i L_0. \tag{16}$$

As the number of generations of asperities tend to infinity, any generation of asperities with a total area less than a critical area A_c will be for a selected load P in plastic deformation. The critical area is related to the yield stress of the material through the relationship

$$\frac{P}{\sigma_y} = \left(\frac{1}{f_x}\right)^n L_0. \tag{17}$$

Solving eqn (17) for n (n being an arbitrary positive integer) gives the relationship

$$n = \begin{cases} 1 + \text{trunc}(\zeta), & \zeta \notin Z, \\ \zeta, & \zeta \in Z, \end{cases} \tag{18a,b}$$

where

$$\zeta = \frac{\ln \xi}{\ln 1/f_x}, \quad \xi = P/L_0\sigma_y, \quad (0 \leqslant \xi \leqslant 1). \tag{19}$$

The function trunc(ζ) takes the value of ζ and truncates it to an integer value.

The total displacement of the Cantor set surface can be represented in terms of the elastic and plastic components of the displacement such that

$$u = u_e + u_p. \tag{20}$$

By letting the number of generations of asperities tend to infinity and simultaneously accounting for volume conservation of the plastically deforming material (Warren *et al.*, 1994), the plastic component of the displacement of the nth generation of asperities can be expressed as

$$u_n = \frac{X\gamma h_0}{f_z^{n-1}}. \tag{21}$$

The parameters X and γ are defined by eqn (A3) in the Appendix. If volume conservation is neglected, the product $X\gamma$ is taken as unity. In the case where volume conservation is not neglected it is assumed that the plastically deformed volume of the nth generation of asperities flows into the troughs between the nth generation of asperities causing the length of the $(n-1)$th generation of asperities to increases by a length $(h_{n-1} - u_n)$. The total displacement of the discrete Cantor set surface including the volume conservation effect can be expressed in dimensionless form as

$$u^* = \left\{ X_\gamma \left(\frac{1}{f_z}\right)^{n-1} + \xi\psi(f_z - X_\gamma)\left(\frac{f_x}{f_z}\right)^{n-1} + \xi\psi(f_z - 1)\sum_{k=0}^{n-2}\left(\frac{f_x}{f_z}\right)^k \right\}, \tag{22}$$

where $u^* = u/h_0$, and $\psi = \sigma_y/E$. The first term on the right-hand side of eqn (22) is the displacement due to the plastic deformation, the second term reflects the elastic deformation of the $(n-1)$th generation of asperities, and the last term is attributed to the elastic deformation of the remaining generations of asperities.

Values of σ_y, E, f_x, f_z, ξ, and n are required to evaluate eqn (22). Here, σ_y and E are material properties, f_x and f_z characterize the structure of the Cantor set model and are related through the fractal dimension D, ξ is the dimensionless form of the applied load, and n defines the current generation of asperities that deforms plastically, and is obtained through the use of eqn (18).

4. CONTINUOUS ELASTIC–PERFECTLY PLASTIC DEFORMATION MODEL

The displacement obtained in eqn (22) is derived in the form of sums, is discrete in nature, and a discontinuous function of the applied load. Because of this, it is of interest to derive a continuous solution for the elastic–perfectly plastic problem and compare the results with the discrete solution in eqn (22).

The plastic component of the displacement can be derived by inverting the expression obtained for the rigid–perfectly plastic problem (Warren *et al.*, 1994) as given by eqn (A5) in the Appendix. It follows that

$$u_p = \phi\left(\frac{\xi}{\theta}\right)^{1/\alpha}, \quad \text{where} \quad \theta = \frac{1}{\alpha}\left(\frac{f_x - 1}{f_z - 1}\right). \tag{23}$$

The parameters ϕ and α are defined by eqns (A2) and (A5) in the Appendix.

The elastic component of the displacement consists of two parts. The first part corresponds to the elastic deformation of the material conserved during the plastic deformation process, and the second part corresponds to the elastic deformation of the remaining material. For the first part it is assumed that the conserved material in the range $u_p \leqslant z \leqslant u_p'$ $(u_p' = u_p/X_\gamma)$ maintains a constant cross-sectional area equal to the area obtained at u_p while taking into account volume conservation. The elastic deformation of the conserved material is

$$u_{e1} = \frac{P}{E}\int_{u_p}^{u_p'} \frac{\mathrm{d}z}{A(u_p)}, \quad \text{where} \quad A(u_p) = L_0\xi. \tag{24}$$

After integration of eqn (24), the first part of the elastic deformation can be expressed in the form

$$u_{e1} = \psi f_z h_0 (1 - X_\gamma)\left(\frac{\xi}{\theta}\right)^{1/\alpha}. \tag{25}$$

For the remaining material it is assumed that (a) the elastic deformation given by eqn (15) can be represented in an integral form, and (b) the cross-sectional area can be approximated using the asymptotic result given by eqn (A7) in the Appendix (neglecting volume conservation). It then follows that

$$u_{e2} = \psi\left(\frac{\xi}{\theta}\right)\int_{u_p'}^{f_z h_0}\left(\frac{z}{f_z h_0}\right)^{-\alpha} dz. \tag{26}$$

Integration of eqn (26) from u_p' to $f_z h_0$ provides two solutions for the second part of the elastic deformation

$$u_{e2} = \begin{cases} \dfrac{\psi f_z h_0}{1-\alpha}\left[\dfrac{\xi}{\theta} - \left(\dfrac{\xi}{\theta}\right)^{1/\alpha}\right], & \alpha \neq 1, \\ -\psi f_z h_0 \xi \ln(\xi), & \alpha = 1. \end{cases} \tag{27a,b}$$

The total displacement is obtained by superimposing eqns (23), (25), and (27), which can be expressed in dimensionless form for $\alpha \neq 1$ as

$$u^* = \left\{X\gamma f_z\left(\frac{\xi}{\theta}\right)^{1/\alpha} + \psi f_z(1-X\gamma)\left(\frac{\xi}{\theta}\right)^{1/\alpha} + \frac{\psi f_z}{1-\alpha}\left[\frac{\xi}{\theta} - \left(\frac{\xi}{\theta}\right)^{1/\alpha}\right]\right\}, \tag{28}$$

and similarly for $\alpha = 1$

$$u^* = \{X\gamma f_z \xi + \psi f_z(1-X\gamma)\xi - \psi f_z \xi \ln(\xi)\}. \tag{29}$$

The logarithmic singularity that occurs at $\xi = 0$ in the last term on the right-hand side of eqn (29) is a weak singularity such that in the limit as $\xi \to 0$ the last term goes to 0. Both the solutions given by eqns (28) and (29) are therefore well behaved for all admissible values of $\alpha > 0$.

5. RESULTS AND DISCUSSION

Numerical results are presented in Fig. 4(a)–(f) for the load–displacement relationship in non-dimensional form for the Cantor set surface profile shown in Fig. 1. The parameters $s = 2$ and $f_x = 1.5$ were held constant, giving a constant Cantor set dimension $D_c = 0.6309$ for this illustrative example. In all cases, the displacements were kept in the same range to illustrate the effect that the applied load has at different fractal dimensions. The selected material properties correspond to AISI 1045 steel, for which the yield strength and Young's modulus are approximately (Shigley and Mitchell, 1984) 700 MPa, and 210 Gpa, respectively. Results are presented with and without volume conservation and the continuous solutions are compared with the discrete solutions. According to both models, a significantly larger load is required to produce the same displacement if the volume is conserved. The results of the continuous solution match those of the discrete model reasonably well (Fig. 4(a),(b)) at the critical load points where a generation of asperities collapse with the continuous solution giving slightly larger displacements. It is further observed that the difference between the two solutions increases with either an increase in load or decrease in fractal dimension. The discrete model data suggests that the displacements at the critical points can be considered to scale as the load to a power greater than one, which is consistent with the results from the continuous solution. Between $D = 1.2$ and 1.3, the value of f_z becomes less than f_x, and the data at the critical load points of the discrete model suggest that the displacement can be considered to scale as the load to a power less than one. This result again is consistent with the results from the continuous solution. However, as the value of D is increased, the displacements of the discrete model at the critical points slightly exceed the continuous solution results for the same value of load. The differences in the results obtained by the two models can be attributed to the asymptotic assumptions made in the development of the continuous model. This result does indicate however that the asymptotic assumptions used in the continuous model provide a reasonable approximation to the discrete model over a wide range of u^*. Furthermore, in reality a real surface may

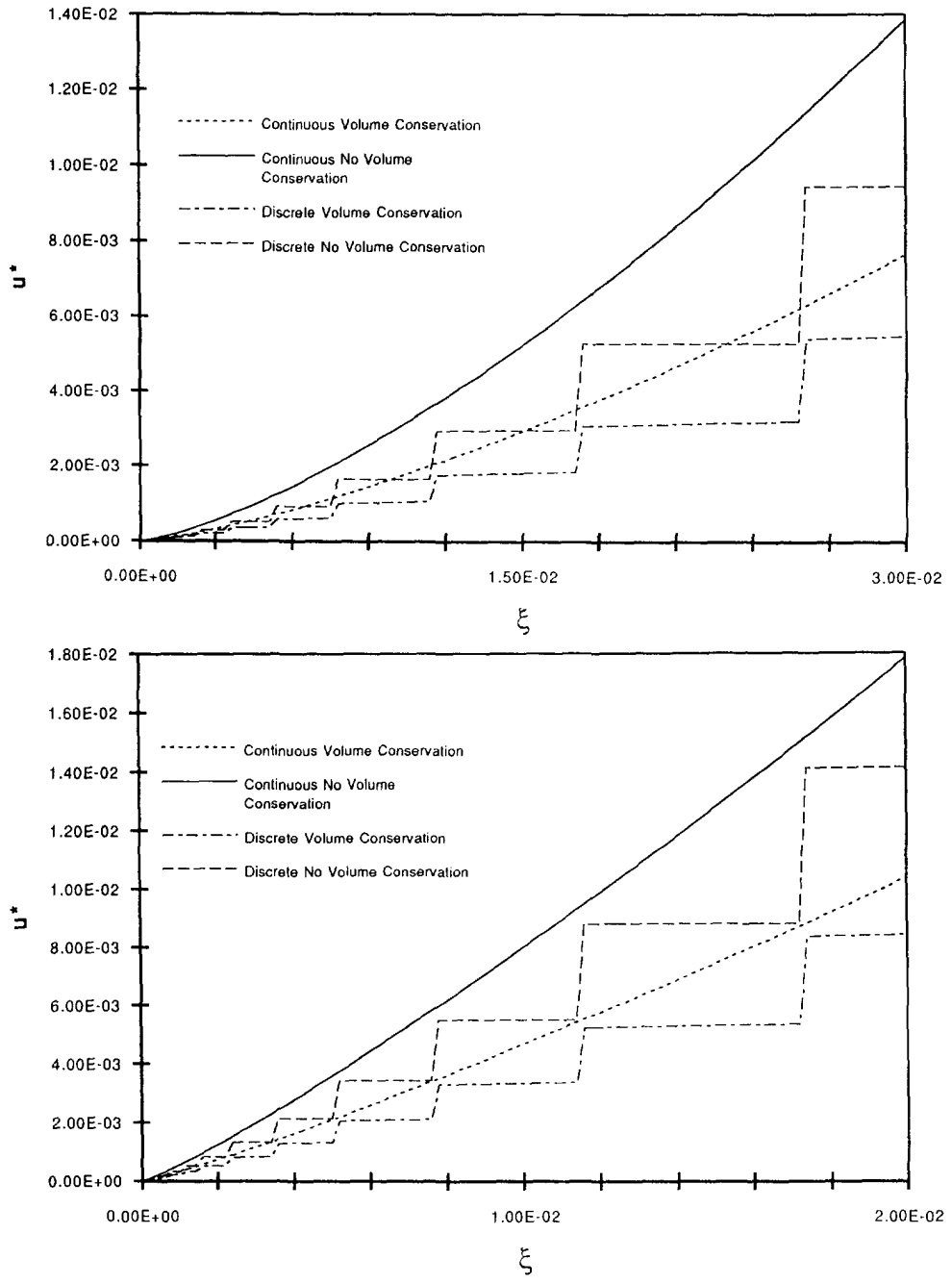

Fig. 4. Non-dimensional load–displacement curves for a Cantor set surface with $s = 2$ and $f_x = 1.5$; (a) $D = 1.1$, (b) $D = 1.2$, and (c) $D = 1.3$; (d) $D = 1.4$, (e) $D = 1.5$, and (f) $D = 1.6$.

not actually be discrete and the continuous model may provide results that are closer to the actual deformation behavior than the discrete model does.

The components of the elastic deformation with volume conservation for both the discrete and continuous models in Fig. 4(b) and (e) are shown in Fig. 5(a) and (b), respectively. In both cases the elastic deformation for the given material, geometry, and loading parameters is much smaller than the plastic deformation and thus contributes very little to the total deformation. In many cases the plastic deformation will most likely be the dominant displacement mode associated with the initial loading of a surface. The amount of elastic deformation exhibited by the Cantor set models is dependent upon the material parameter ψ, the two geometric parameters f_x and f_z, and the loading variable ξ. Examination of eqns (22), (28), and (29) shows that the elastic component of displacement varies

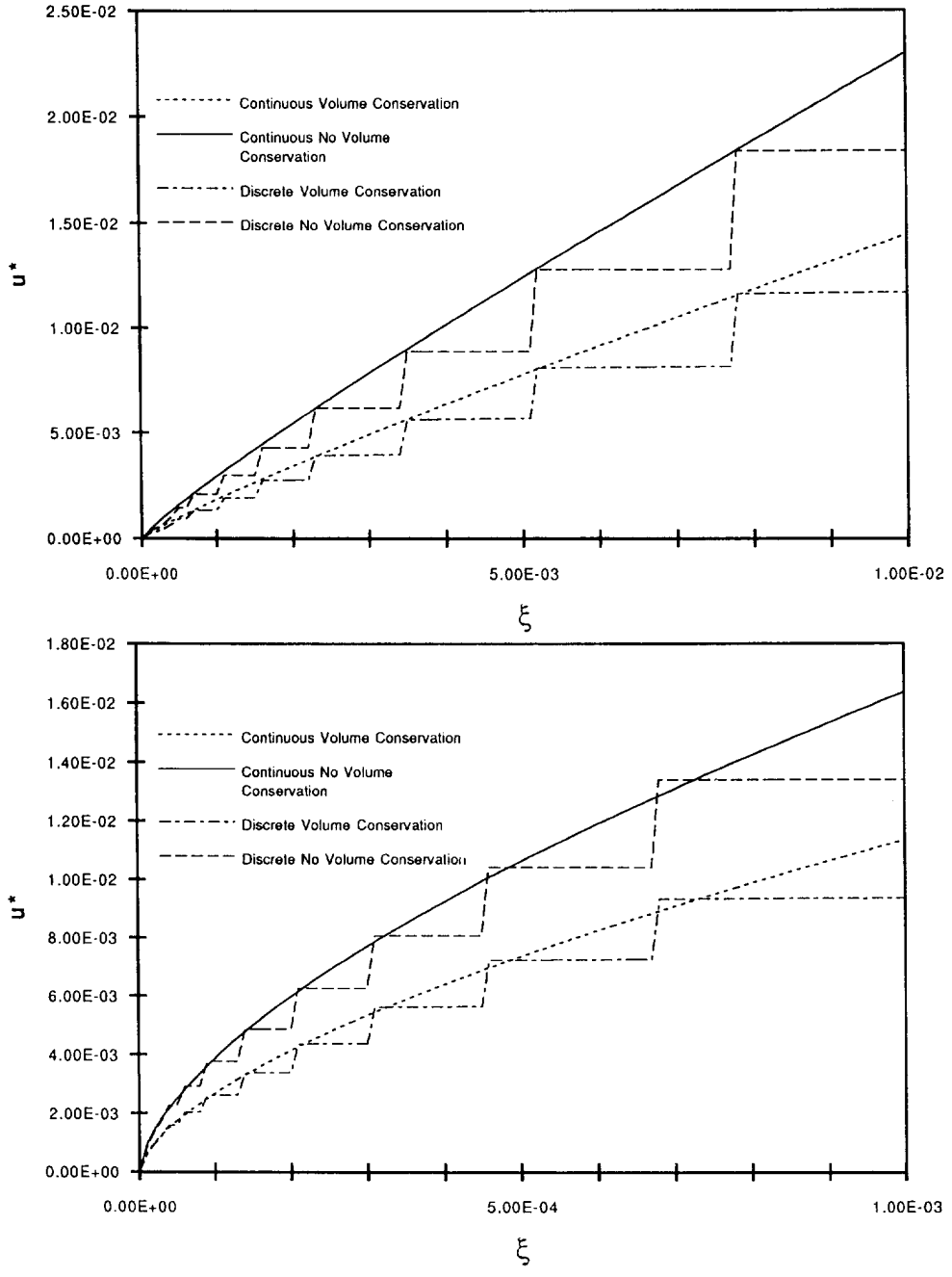

Fig. 4. *Continued.*

linearly with changes in ψ. To examine the effects of geometry and load, the individual components of displacement that account for volume conservation are plotted as functions of the fractal dimension D for several values of dimensionless load ξ while the other parameters are held constant. In Fig. 6 (a), (b), and (c), the dimensionless load is taken as 1×10^{-6}, 1×10^{-4}, and 1×10^{-2}, respectively, while $s = 2$, $D_c = 0.6309$, and $\psi = 3.33 \times 10^{-3}$. It is observed that the elastic component of displacement contributes less to the total displacement as the fractal dimension D is increased for all considered values of ξ. For small values of ξ it is seen that the elastic component of displacement is dominant for low values of D (Fig. 6(a)), and in fact as $\xi \to 0$ the elastic component of displacement exceeds in magnitude the plastic component for values of D in which f_z is less than f_x. However, as D is increased the plastic component of displacement increases, and in fact becomes the dominant deformation mode. Similar trends are displayed in Fig. 6(b). However, at much

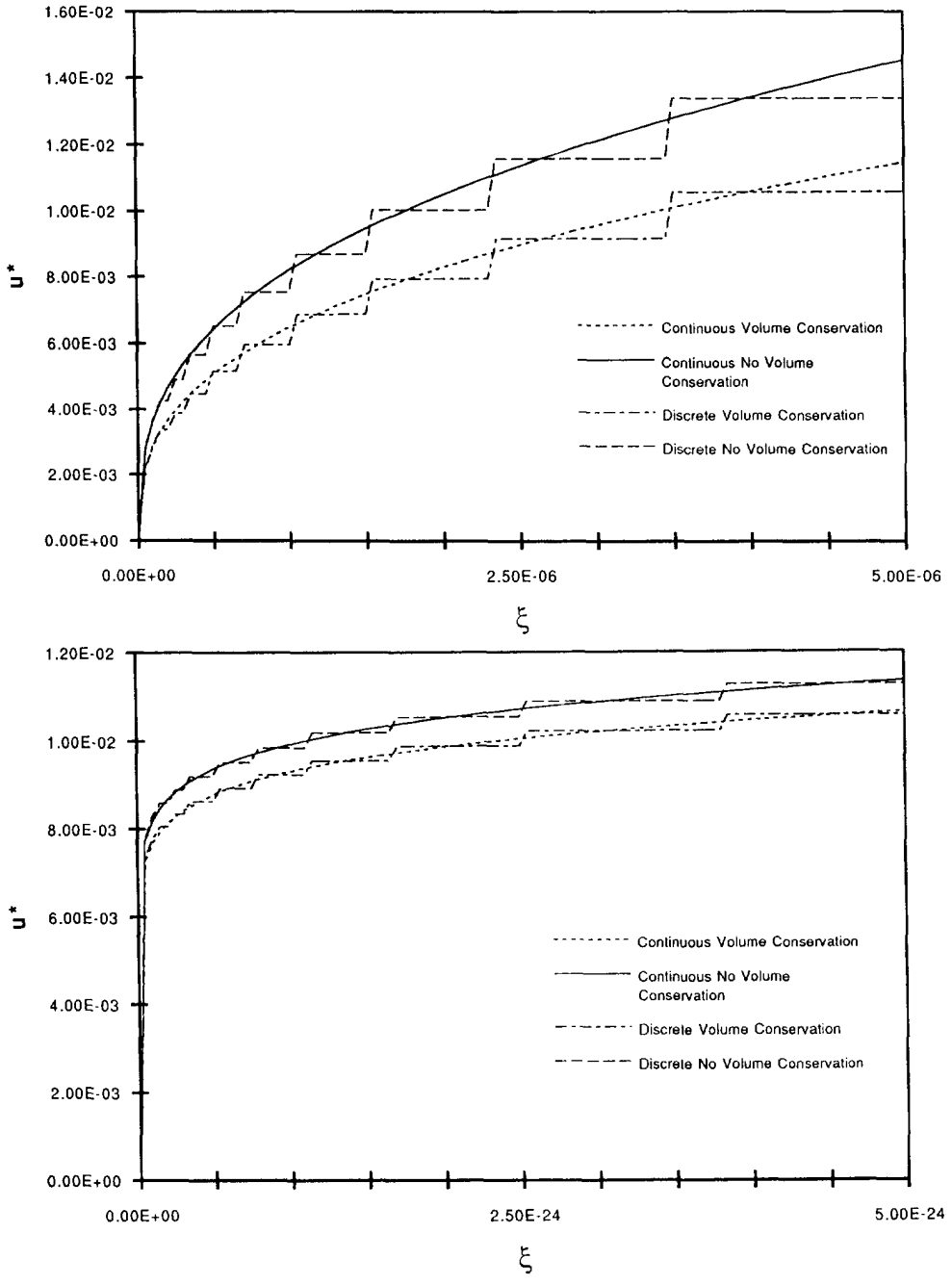

Fig. 4. *Continued.*

higher loads the elastic component of displacement always remains less than the plastic component for all values of D (Fig. 6(c)). These results indicate that the component of plastic deformation grows exponentially with decreasing f_z, and becomes orders of magnitude greater than the elastic component. This elastic component grows much slower, and in some cases decreases for surfaces with large D. A decrease in f_z physically corresponds to an increase in the length of all $(n+1)$th generations of asperities and leads to an increase in the fractal dimension D when the parameters s and f_x are held fixed. This result is consistent with curves that exhibit fractional Brownian motion as discussed by Voss (1988), where the surface becomes rougher with sharper peaks when the fractal dimension D is increased. Therefore, higher fractal dimensions give rise to more sharply peaked asperities which deform plastically at lower loads as predicted by both of the present Cantor set models.

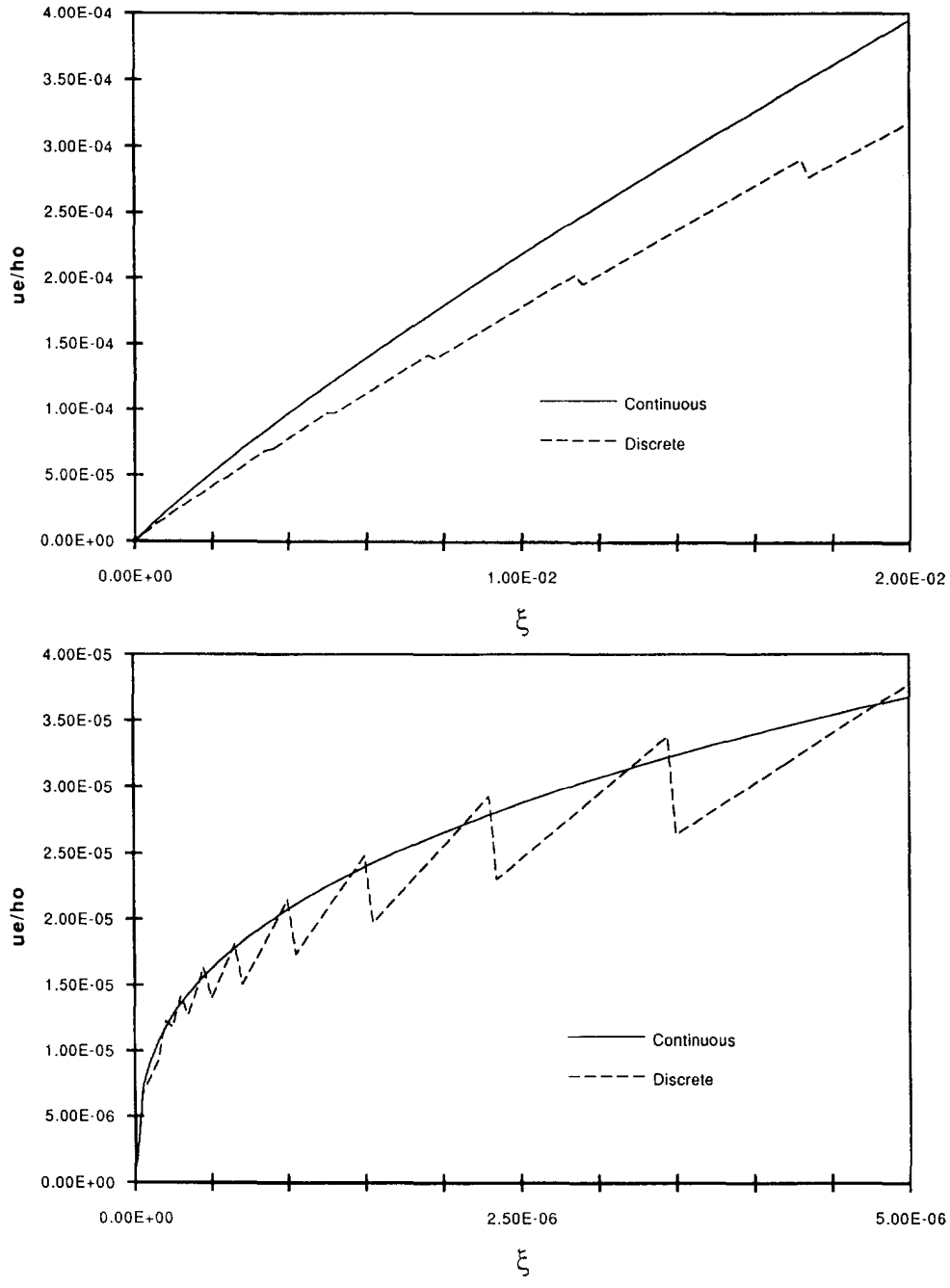

Fig. 5. Dimensionless values of the elastic component of displacement plotted as a function of dimensionless load P/P_0 with $s = 2$ and $f_s = 1.5$; (a) $D = 1.2$ and (b) $D = 1.5$.

Due to the periodicity of the Cantor set surface, it is doubtful that either of the considered models will provide an exact representation of the surface structure. However, these models do provide a further insight into the surface structure and its effect on the deformation process. In an averaged sense, these models appear to provide reasonable results. Specifically, both models provide (a) an estimate of the error associated with neglecting volume conservation, which is common with many current surface deformation models, and (b) an estimate of the elastic and plastic deformation that occurs and their relationship to the applied load, material properties, and geometric structure of the surface. A numerical measure of the error associated with neglecting volume conservation can be obtained by considering the ratio of the displacement with volume conservation (vc) over the displacement neglecting volume conservation (nvc). If the plastic component of

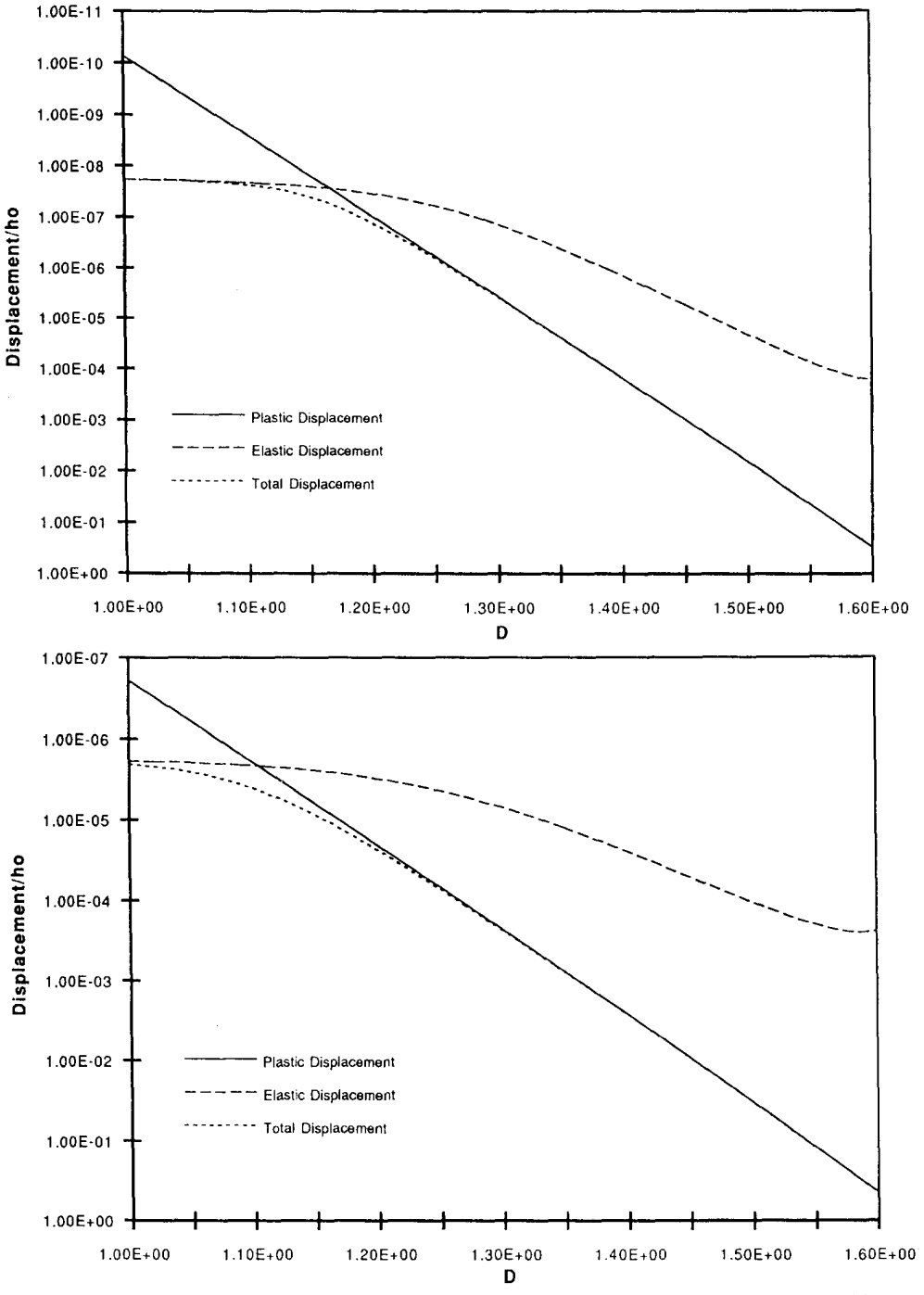

Fig. 6. The dimensionless displacement u/h_0 is plotted as a function of the fractal dimension D, with $s = 2$, $D_c = 0.6309$, and $\psi = 3.33 \times 10^{-3}$ held constant at the dimensionless loads (a) 1×10^{-6}, (b) 1×10^{-4}, and (c) 1×10^{-2}.

displacement is much larger than the elastic component, the latter can be neglected and the effect of the volume conservation is reflected in the ratio $u^*_{rc}/u^*_{nrc} = 1/\kappa^{1/\alpha}$ where κ is given by eqn (A8) in the Appendix. This result holds for both the discrete and continuous models.

Recent experimental work by Handzel–Powierza *et al.* (1992) has shown that the load–displacement relationships for face turned, ground, and bead-blasted carbon steel specimens (0.45% carbon) follow a sigmoidal curve similar to that in Fig. 7. The experimental data obtained by Handzel–Powierza *et al.* (1992) for the ground specimen are compared in Fig. 7 with the theoretical prediction computed from eqn (28). The error associated with the

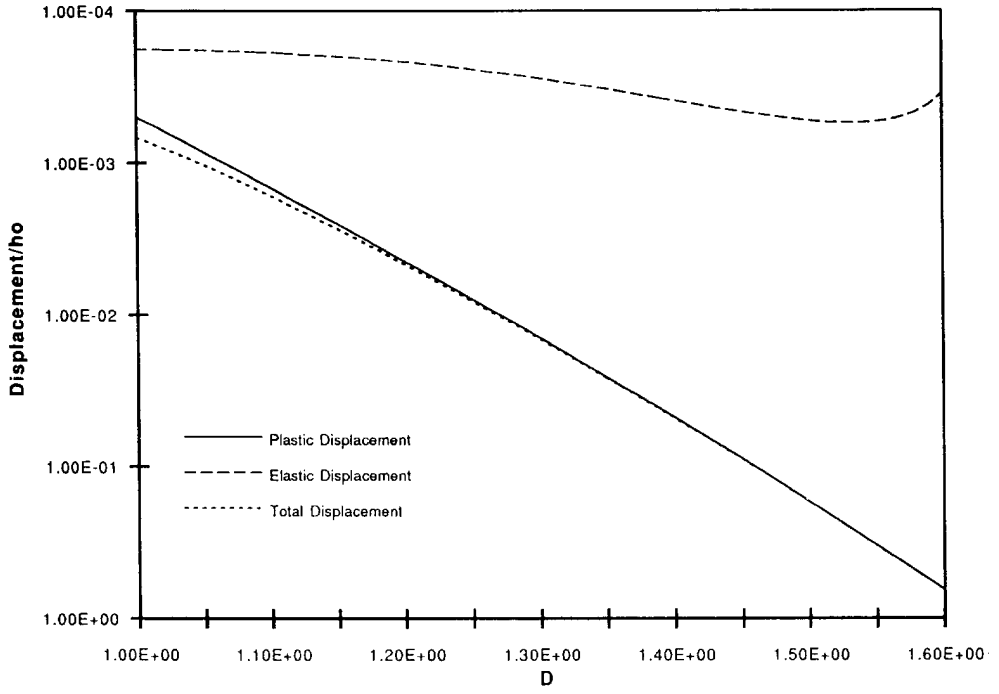

Fig. 6. *Continued.*

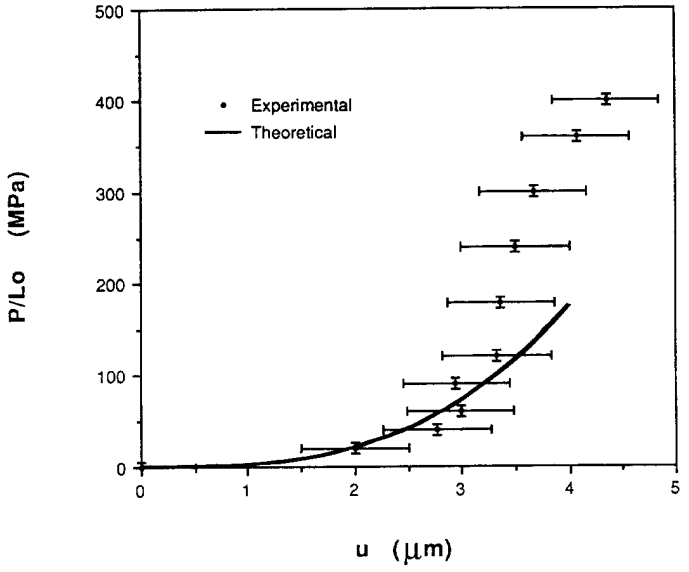

Fig. 7. Experimental and theoretical load–displacement results for a ground medium carbon steel specimen.

experimental measurements was determined by Handzel–Powierza *et al.* (1992) to be approximately ± 0.5 μm for the displacements, and ± 5 MPa for the load. In the early stages of deformation, the load scales as the displacement raised to a power greater than one. In the later stages, the load–displacement curve changes direction, and the load scales as the displacement raised to a power less than one, which is consistent with models based on the plastic deformation of bulk material. In Handzel–Powierza *et al.* (1992) the test data in the early stages of deformation are compared with a modified version of the G&W model that considers only elastic deformation of asperities. However, according to the results of the elastic–perfectly plastic models, it is highly probable that during the first loading in the early stages of deformation both plastic and elastic deformation of asperities exist, with the

plastic deformation possibly being much greater than the elastic deformation. With this in mind, it is observed that the discrete elastic–perfectly plastic Cantor set model can indeed be employed to simulate the contact deformation in the early stages. As shown in Fig. 7, reasonably good agreement between the theoretical and experimental results exists in the early stages of loading. For this rough theoretical estimate, the material properties were again taken as that for AISI 1045 steel. It was further assumed that the profile fractal dimension is $D = 1.5$, which appears to be reasonable based on the results obtained by Majumdar *et al.* (1991) for ground stainless steel surfaces, which were found to exhibit surface profiles with a fractal dimension of $D = 1.5$. The corresponding Cantor set dimension was assumed to be $D_c = 0.6228$ with $s = 3$, giving $f_x = 1.9455$ and $f_z = 1.2418$. The depth h_0 was taken as 6.6 μm which corresponds to twice the r.m.s. height as given by Handzel-Powierza *et al.* (1992).

Using modern surface roughness measuring instruments such as stylus profilometers, optical interferometers, scanning tunneling microscopes, and atomic force microscopes, it is possible to determine whether a surface is fractal or not (Majumdar *et al.*, 1991). If the surface is fractal, the self-affine fractal dimension D can be determined from the measured data along with the corresponding values of the parameters h_0, L_0. By considering a large number of cross-sectional areas of surface profiles, averaged values of the parameters f_x and f_z can be determined from eqn (A7) in the Appendix. Using these averaged values of f_x and f_z, eqns (28) or (29) can be employed to provide an estimate of the load–displacement relationship, and to give some idea of the amount of elastic and plastic deformation expected at a desired load.

In conclusion, all geometrical parameters of the proposed model can be directly, if only approximately, determined from the measured surface roughness. Force–displacement relationships are derived in a closed form allowing for simple parametric studies of the influence of surface roughness through the fractal dimension D and volume conservation during plastic deformation. The computed results are in very good agreement with experimental data within the range for which bulk plasticity is not a dominant factor.

Acknowledgements—The authors gratefully acknowledge financial support rendered by the research grant awarded by the National Science Foundation, Division of Engineering, Solid Mechanics Program to the Arizona State University which made this work possible. The authors also gratefully acknowledge the constructive comments from the reviewers.

REFERENCES

Archard, J. F. (1957). Elastic deformation and the laws of friction. *Proc. R. Soc.* **A243,** 190–205.
Bhushan, B. (1990). *Tribology and Mechanics of Magnetic Storage Devices*. Springer, New York.
Bhushan, B. and Majumdar, A. (1992). Elastic–plastic contact model for bifractal surfaces. *Wear* **153,** 53–64.
Borodich, F. M. and Mosolov, A. B. (1991). Fractal contact of solids. *Sov. Phys. Tech. Phys.* **36**(9), 995–997.
Borodich, F. M. and Mosolov, A. B. (1992). Fractal roughness in contact problems. *J. Appl. Maths. Mech.* **56**(5), 681–690.
Bowden, F. P. and Tabor, D. (1964). *Friction and Lubrication of Solids*, Parts I and II. Clarendon Press, Oxford.
Chang, W. R., Etsion, I. and Bogy, D. B. (1987). An elastic–plastic model for the contact of rough surfaces. *ASME J. Tribology* **109,** 257–263.
Cook, R. D. and Young, W. C. (1985). *Advanced Mechanics of Materials*. Macmillan Publishing Co., New York.
Greenwood, J. A. and Williamson, J. B. P. (1966). Contact of nominally flat surfaces. *Proc. R. Soc.* **A295,** 300–319.
Handzel-Powierza, Z., Klimczak, T. and Polijaniuk, A. (1992). On the experimental verification of the Greenwood–Williamson model for the contact of rough surfaces. *Wear* **154,** 115–124.
Hill, R. (1950). *The Mathematical Theory of Plasticity*. Clarendon Press, Oxford.
Johnson, K. L. (1985). *Contact Mechanics*. Cambridge University Press, Cambridge.
Liu, S. H., Kaplan, T. and Gray, L. J. (1986). Theory of the AC response of rough interfaces. In *Fractals in Physics* (Edited by L. Pietronero and E. Tosatti), pp. 383–389. North-Holland, New York.
Majumdar, A. and Bhushan, B. (1991). Fractal model of elastic–plastic contact between rough surfaces. *ASME J. Tribology* **113,** 1–11.
Majumdar, A., Bhushan, B. and Tien, C. L. (1991). Role of fractal geometry in tribology. *Adv. Inform. Storage Syst.* **1,** 231–266.
Mandelbrot, B. B. (1982). *The Fractal Geometry of Nature*. Freeman, San Francisco.
Mandelbrot, B. B. (1985). Self-affine fractals and fractal dimension. *Phys. Scr.* **32,** 257–260.
Shigley, J. E. and Mitchell, L. D. (1984). *Mechanical Engineering Design*. McGraw Hill, New York.
Voss, R. F. (1988). Fractals in nature: from characterization to simulation. In *The Science of Fractal Images* (Edited by H. O. Pietgen and D. Saupe), pp. 21–70. Springer-Verlag, New York.
Warren, T. L., Majumdar, A. and Krajcinovic, D. (1994). A fractal model for the rigid–perfectly plastic contact of rough surfaces. *J. Appl. Mech.* (accepted).

APPENDIX

Rigid–perfectly plastic deformation model

The incremental change in load divided by the incremental change in displacement in going from the $(n+1)$th generation to the nth generation of asperities (Warren *et al.*, 1994) is

$$\frac{\Delta P_{n+1}}{\Delta u_{n+1}} = \frac{P_0(f_x-1)}{\phi(f_z-1)}\left(\frac{f_z}{f_x}\right)^{n+1}, \tag{A1}$$

where

$$P_0 = \sigma_y L_0, \quad \phi = X\gamma f_z h_0, \tag{A2}$$

$$X = \left(1-\frac{1}{f_x}\right), \quad \gamma = \frac{1}{\left(1-\frac{1}{f_z f_x}\right)}. \tag{A3}$$

In eqn (A2), σ_y denotes the yield stress of the material. The geometric series which defines γ in eqn (A3) always converges since the geometric constraints require that $f_x > 1$ and $f_z > 1$. The expressions for X and γ in eqn (A3) are due to volume conservation during plastic deformation. If volume conservation is neglected, $\phi = f_z h_0$.

In the limit as $(n+1) \to \infty$, eqn (A1) can be expressed as the asymptotic derivative

$$\frac{dP}{du} = \frac{P_0(f_x-1)}{\phi(f_z-1)}\left(\frac{u}{\phi}\right)^{(\ln f_x/\ln f_z)-1}. \tag{A4}$$

The asymptotic load–displacement relationship for a rigid–perfectly plastic fractal surface is derived by integrating eqn (A4) subject to the initial condition that $P = 0$ for $u = 0$. Thus (Warren *et al.*, 1994)

$$P = \frac{P_0}{\alpha}\left(\frac{f_x-1}{f_z-1}\right)\left(\frac{u}{\phi}\right)^{\alpha}, \quad \text{where} \quad \alpha = \frac{\ln f_x}{\ln f_z}. \tag{A5}$$

The solution (A5) is based on asymptotic behavior [see also Borodich and Mosolov (1991,1992)], and will give the best results if $u \ll h_0$. The exponent α in eqn (A5) used in conjunction with eqn (13), provides the relationship

$$\alpha = \frac{1-D_c}{1+D_c-D}, \tag{A6}$$

where $\alpha \geqslant 0$, and is represented in terms of the fractal dimension D and the Cantor set dimension D_c.

Dividing eqn (A5) by σ_y gives the actual linear area of contact at any displacement u. Taking $\phi = f_z h_0$ corresponds to neglecting volume conservation. The linear area displacement relationship in this case is equal to

$$A_{nvc} = \frac{L_0}{\alpha}\left(\frac{f_x-1}{f_z-1}\right)\left(\frac{u}{f_z h_0}\right)^{\alpha}. \tag{A7}$$

Evaluating eqn (A7) at two separate values of u and equating the corresponding values of A_{nvc} with the linear area from an experimentally obtained surface profile (at respective distances u below the r.m.s. height σ as shown in Fig. 2) provides two equations which can be solved to determine the geometric parameters f_x and f_z. This process should be carried out over a large number of realizations in order to obtain statistically valid values of f_x and f_z. These averaged values of f_x and f_z can then be used in conjunction with eqn (13) to obtain the value of s that provides a spatial distribution of the asperities. The load–displacement relationship given in eqn (A5) can be characterized from this result without using the fractal dimension D. However, the relationship between f_x and f_z and D provides further insight into the changes in geometric structure of the modeled surface profile with length scale.

A measure of the error involved with neglecting volume conservation during plastic contact can be derived by considering the ratio of the applied load for the volume conservation model to the applied load for the model without volume conservation. Denoting this ratio by κ it is found that

$$\kappa = \left(\frac{1}{X\gamma}\right)^{\alpha}, \tag{A8}$$

where $\kappa > 1$ is entirely dependent upon the geometric parameters f_x and f_z.